Cerebellar Tissue Strain in Chiari Malformation with Headache

Bryden H. Dawes[1], Robert A. Lloyd[2], Jeffrey M. Rogers[1,3], John S. Magnussen[1], Lynne E. Bilston[2], Marcus A. Stoodley[1]

■ OBJECTIVE: **The pathogenesis of Chiari malformation type 1 (CM-1)—associated Valsalva headache is unknown, but it may be caused by abnormal cerebellar tonsil tissue strain. Advances in cardiac-gated magnetic resonance imaging (MRI) techniques such as balanced fast-field echo (bFFE) allow quantification of the motion of anatomic structures and can be used to measure tissue strain. The current study investigated the relationship between Valsalva heachache and tonsillar motion in patients with CM-1.**

■ METHODS: **A retrospective review of patients with CM-1 who had undergone cardiac-gated bFFE MRI was performed. Headache symptoms were retrieved from the medical records. Anatomic landmarks were manually selected on the cine bFFE, and a validated motion-tracking software was used to assess motion over the cardiac cycle in patients at rest. For each patient, displacement, strain, and strain rate were calculated for 3 anatomic segments. Patients undergoing surgery were examined before and after surgery.**

■ RESULTS: **From 88 patients, a total of 108 bFFE sequences were analyzed. Valsalva headache was present in 50% of patients. Cerebellar tonsil displacement ($P = 0.003$), strain ($P = 0.012$), and maximum strain rate ($P = 0.04$) were reduced after surgery (n = 20). There was no statistically significant association between tissue motion and headache symptoms.**

■ CONCLUSION: **The results of this study do not support a relationship between cardiac cycle cerebellar strain and Valsalva headache in patients with CM-1. It is possible that cerebellar strain related to respiratory maneuvers is associated with headache in Chiari patients. Further investigation of tissue strain is warranted because it represents a potential biomarker for outcomes after surgery.**

INTRODUCTION

Chiari malformation type 1 (CM-1) is an abnormality of the craniocervical junction. It is often defined as caudal descent of the cerebellar tonsils >5 mm below the foramen magnum.[1-3] However, this is regarded by many as too simplistic to be a diagnostic criterion.[4-7] Whereas CM-1 may be asymptomatic,[2] the most prevalent presenting symptom is headache, commonly in the occipital and posterior cervical regions.[3,8] Typically, there is paroxysmal pain in the occipital region associated with laughing, sneezing, coughing, or a forward bending posture,[3] termed Valsalva or tussive headache.

The pathogenesis of Valsalva headache in CM-1 is not known. Potential mechanisms include compression of the C1 and C2 nerve roots by the descending tonsils,[9,10] transient craniospinal pressure dissociation,[11,12] increased cerebrospinal fluid (CSF) pressure,[13] and reduced CSF compliance[3] secondary to reduced posterior fossa CSF volume. These hypotheses fail to explain the spectrum of radiologic and clinical presentations. Defining the pathophysiology underpinning CM-1–related Valsalva headache would have a direct clinical application and would be useful in guiding treatment decisions and assessing patient outcomes.

Patients with CM-1 have abnormal CSF flow dynamics[14-16] and altered motion of the neural structures at the craniocervical junction during the cardiac cycle.[17] Motion of these structures

Key words
- Balanced fast-field echo
- Cerebellar tonsils
- Chiari malformation
- Cine magnetic resonance imaging
- Craniocervical junction

Abbreviations and Acronyms
bFFE: Balanced fast-field echo
CSF: Cerebrospinal fluid
CM-1: Chiari malformation type 1
DTI: Diffusion tensor imaging
ICC: Interclass correlation coefficient
MRI: Magnetic resonance imaging
PFD: Posterior fossa decompression

From the [1]Department of Clinical Medicine, Macquarie University, Sydney; [2]Neuroscience Research Australia and Prince of Wales Clinical School, University of New South Wales, Sydney; and [3]Faculty of Health Sciences, University of Sydney, Sydney, New South Wales, Australia

To whom correspondence should be addressed: Marcus A. Stoodley, Ph.D. [E-mail: marcus.stoodley@mq.edu.au]

Citation: World Neurosurg. (2019) 130:e74-e81.
https://doi.org/10.1016/j.wneu.2019.05.211

Journal homepage: www.journals.elsevier.com/world-neurosurgery

Available online: www.sciencedirect.com

encompasses both displacement and stretch, termed strain. A relationship between cardiac cycle tonsil tissue strain and Valsalva headache in CM-1 has previously been suggested.[17] The investigators assessed patients at rest and not during Valsalva manuevers. Tissue strain provides a potenetial explanation for Valsalva headache in CM-1, via stretching of cerebellar tonsil perivascular sensory fibers, or affecting cerebellar connections to supratentorial structures.

Magnetic resonance imaging (MRI) techniques are used to investigate CM-1 and abnormalities of the craniocervical junction. Conventional imaging displays intracranial structures as static, not demonstating the movement that occurs with the cardiac and respiratory cycles. Recent MRI advances provide dynamic imaging, allowing tissue movement to be assessed.[18,19] Balanced fast-field echo (bFFE) is a type of balanced steady-state free precession imaging. The technique provides cardiac-gated cine T2-weighted images and can be used to image the midsagittal plane at multiple time points. This allows dynamic assessment of anatomic structures throughout the cardiac cycle.[20]

Using cardiac-gated bFFE MRI, we aimed to assess the cerebellar motion and determine its relationship to both Valsalva and non-Valsalva headache in patients with CM-1. The primary aim of the study was to assess the relationship of tonsil strain and Valsalva headache. Secondary objectives included assessment of tonsil motion and its relationship to symptoms, including Valsalva and non-Valsalva headache, along with the effect of surgery on tonsil motion and cerebellar strain. We hypothesized that the cause of Valsalva headache may be related to increased cerebellar tonsil strain and that surgery would be associated with both reduced tonsil strain and Valsalva headache symptoms.

METHODS

A retrospective review was conducted of all CM-1 patients who had undergone a cine bFFE sequence MRI of the craniocervical junction at Macquarie University Hospital. This study was approved by the Human Research Ethics Committee of Macquarie University.

Participants

Patients were eligible for inclusion if they had CM-1, defined as cerebellar ectopia >5 mm below the foramen magnum. This criterion was adopted for simplicity and reproducibility, although we recognize that it may not encompass the full spectrum of CM. We did not differentiate between CM-1 and so-called Chiari 1.5.

Both nonoperative and operative patients were included. Patients were excluded if they had undergone previous surgery at the craniocervical junction. Patients with poor bFFE image quality due to either low signal-to-noise ratio, tissue contrast, or image inhomogeneity were excluded from the study.

Clinical data were obtained through review of the medical records. For each patient, baseline characteristics including age, gender, and the presence of Valsalva and non-Valsalva headaches were obtained. Evaluation of the clinical outcomes after surgery occurred at the first follow-up clinic visit, generally 6 to 12 weeks after surgery.

Patients were grouped according to clinical symptoms and operative status. Symptom status was defined based on the presence and type of headache: no headache, non-Valsalva headache, and Valsava headache. Operative status included preoperative and postoperative, with preoperative and postoperative imaging paired for analysis.

The indications for surgery included symptomatic CM-1, with Valsalva or non-Valsalva headache, and/or syringomyelia failing conservative management. Operative management consisted of suboccipital craniectomy, C1 laminectomy, and duroplasty with a pericranial or polytetrafluoroethylene graft. The cerebellar tonsils were shrunk by bipolar cautery if necessary to achieve adequate decompression of the craniocervical junction. All procedures were performed by the senior author.

Imaging

A standardized imaging protocol of the craniocervical junction including bFFE sequence was instituted at Macquarie University Hospital in 2011. All examinations were performed on a 3-Tesla MRI scanner (Magnetom Trio, Siemans, Germany). Cardiac gating was performed by either electrocardiography or pulse oximetry. The bFFE technique was used to generate T2-weighted, 4-mm-thick, midsagittal images of the posterior fossa and craniocervical junction. A sequence of 20 or 25 frames was collected across the cardiac cycle.

Image Processing, Data Collection, and Analysis

An uncompressed video was constructed from the raw digital imaging and communications in medicine images in ImageJ (v1.8.0, National Institutes of Health, Bethesda, MD). Anatomic landmarks were manually selected on the first frame by a single blinded investigator. These points were automatically tracked frame to frame using a feature-tracking (Kanade-Lucas-Tomasi) algorithm provided in the Matlab Computer Vision Systems Toolbox (v8.6, TheMathWorks Inc., MA). To verifiy the reliability of the tracking, 10 patients previously analyzed manually by Leung et al.[17] were reanalyzed, and the agreement of the measurements was assessed.

Three anatomic landmarks were selected in each patient (**Figure 1**): the superior aspect of the cerebellar vermis (Sup); the fastigium of the fourth ventricle (IV); and the tip of the cerebellar tonsils (Ton). These landmarks were used to calculate the length (Equation 1) of 3 segments of the cerebellum over each phase of the cardiac cycle: the fastigium to the tip of the tonsils (IV-Ton); the superior aspect of the cerebellum to the fastigium (Sup-IV); and the superior aspect of the cerebellum to the tip of the tonsils (Sup-Ton). To account for intraobserver error, the points were redefined and tracked 3 times, taking an average for subsequent analysis. Tracking was visually inspected on cine bFFE to confirm proper tracking.

$$l = \sqrt{(x_2 - x_1)^2 + (y_2 - y_1)^2} \qquad \text{(Equation 1)}$$

$$\Delta l(t) = l(t) - l_{ref} \qquad \text{(Equation 2)}$$

$$\varepsilon(t) = \sum \frac{\Delta l(t)}{l} \qquad \text{(Equation 3)}$$

$$\dot{\varepsilon}(t) \approx \frac{\varepsilon(t + \Delta t) - \varepsilon(t - \Delta t)}{2\Delta t} \qquad \text{(Equation 4)}$$

Tissue displacement ($\Delta l(t)$: Equation 2) was calculated over the cardiac cycle relative to the segment length at the beginning of systole (l_{ref}). The strain throughout the cardiac cycle was

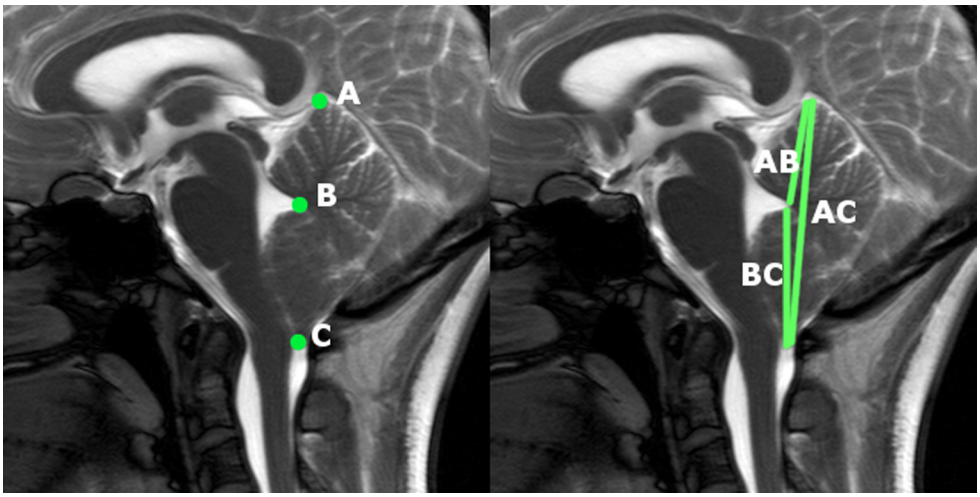

Figure 1. Illustration of the anatomic landmarks and segments on a midsagittal balanced fast-field echo magnetic resonance image of a patient with a Chiari I malformation. (**A**) superior aspect of the cerebellar vermis. (**B**) Fastigium of the fourth ventricle. (**C**) Tip of the cerebellar tonsil. AB = line from the superior aspect of the cerebellar vermis to the fastigium of the fourth ventricle; AC = line from the superior aspect of the cerebellar vermis to the tip of the cerebelllar tonsil; BC = line from the fastigium of the fourth ventricle to the tip of the cerebellar tonsil.

calculated by summing the strains over each measured phase of the cardiac cycle ($\varepsilon(t)$; Equation 3). Strain rate ($\dot{\varepsilon}(t)$) was approximated by the central difference of the strain data (Equation 4). For each cerebellar segment, the maximum displacement, the maximum strain, and the maximum and minimum strain rates were compared.

Variations in resolution and R-R interval time step were accounted for in the data acquisition programming. A subset of images lacked the R-R interval time step, resulting in inability to calculate the duration of the cardiac cycle or strain rate. These patients were excluded from the strain rate analysis.

Statistical Analysis

Statistical analysis was conducted in IBM SPSS Statistics (v24, IBM Corp, Armonk, NY). The agreement of the tracking algorithm and data of Leung et al.[17] was evaluated by calculating the interclass correlation coefficient (ICC) and the 95% confidence interval. The ICC was calculated based on a single-rater, absolute-agreement, 2-way mixed-effect model. χ^2 tests were used to compare symptom rates between groups. To account for nonnormal distributions of data, nonparametric tests were used for further comparisons. Comparisons between patients by headache status (no headache, non-Valsalva headache, Valsalva headache) were conducted with a Kruskal-Wallis test. The effect of surgery was assessed using paired data (before and after operation) and the Sign test. In all analyses, statistical significance was defined as $P < 0.05$.

RESULTS

Participants

In all, 124 CM-1 patients were identified, including 28 males (23%) and 96 females (77%). Of those, 36 patients were excluded because of poor image quality, precluding accurate measurement by use of the motion-tracking algorithm.

In total, 88 patients were included in the final analysis (**Table 1**). Of those, 47 patients (53%) were treated nonoperatively and 41 patients (47%) underwent posterior fossa decompression (PFD). Tonsil coagulation was performed in 3 patients (7%). Within the operative group, postoperative bFFE MRI imaging was available in 20 patients (49%). Among the remaining surgical patients, 11 patients (27%) had external follow-up imaging with no bFFE sequence, 8 patients (20%) were excluded because of poor image quality, and 2 patients (5%) had no available clinical or radiologic follow-up. None of the patients who underwent tonsil coagulation were included in the postoperative analysis group because bFFE imaging was not available.

Seventy-three patients (82%) had headache, of whom 44 patients (50%) had Valsalva headache on presentation. Of the 24 patients with Valsalva headaches who underwent surgery, 19 patients (79%) experienced improvement in Valsalva headache, and symptoms remained unchanged in 2 patients and 2 patients had worsening of Valsalva headache. Within this group, no follow-up clinical data were available for 1 patient.

Of the patients who had worsening of Valsalva headache after surgery, 1 patient had concurrent idiopathic intracranial hypertension and required a ventriculoperitoneal shunt, and the other patient had intracranial hypotension from a spontaneous spinal CSF leak that responded well to lumbar epidural blood patch.

Syringomyelia was present in 9 patients (19%) in the nonoperative group and 15 patients (37%) in the operative group. An improvement in the size of syrinx was seen in 13 patients (87%) after surgery. The syrinx size remained unchanged in 1 patient, and no clinical data were available for another.

Table 1. Summary of Patient Demographics and Clinical Data

Characteristic	Nonoperative	Operative
Number of patients	47	41
Age, years*	37.3 ± 13.2	34.0 ± 11.6
Gender, M:F	10:37	11:30
Headache†	40 (85)	33 (80)
Cerebellar ectopia, mm*	8.3 ± 2.4	10.3 ± 4.1
Syrinx†	9 (19)	15 (37)
Improvement in syrinx†	-	13 (87)
Valsalva headache†	20 (43)	24 (59)
Improvement in Valsalva headache†	-	18 (75)

*Mean ± standard deviation.
†n (%).

Verification

The automated feature tracking correlated with the manually assessed data,[17] (ICC = 0.888, 95% confidence interval 0.448–0.974). The greatest deviation between the 2 methods was attributed to an observer error and a fault in the previous tracking protocol that limited the ability to distinguish motion close to static areas of high grey scale intensity.

Displacement and Strain

The median displacement from the fastigium of the fourth ventricle to the tip of the tonsils in the Valsalva headache, non-Valsalva headache, and no headache groups was 0.48 mm (0.27–0.77 mm), 0.27 mm (0.15–0.66 mm) and 0.38 mm (0.17–0.92 mm), respectively (Table 2). No statistically significant difference was found between headache groups in the IV-Ton segment ($P = 0.21$) or other segments (Table 3).

Maximum tissue strain from the fourth ventricle to the tonsil tip in the Valsalva headache, non-Valsalva headache, and no headache groups was 1.25% (0.77–2.13%), 0.73% (0.40–1.96%) and 1.05% (0.50–2.60%), respectively. No statistical significance between headache groups was demonstrated in the IV-Ton segment ($P = 0.20$) or other segments.

Within the operative group there was a significant reduction in the displacement in the tonsil segment (IV-Ton) after surgery to 0.18 mm (0.13–0.33 mm) ($P < 0.003$) (Table 4). There was also a reduction in the Sup-Ton segment displacement after surgery ($P = 0.012$).

Tonsil strain (IV-Ton) improved to 1.06% (0.58 to 1.78%) after surgery ($P < 0.012$), and there was a reduction in strain in the Sup-Ton segment ($P < 0.012$). Figure 2 shows a comparison of box plots of preoperative and postoperative patients.

Strain Rate

Minimum and maximum strain rates were calculated for all patients. There was a trend toward a difference between headache groups in the IV-Ton segment in both maximum strain rate ($P = 0.06$) and minimum strain rate ($P = 0.07$); however, statistical significance was not achieved. After surgery there was a reduction in the maximum strain rate in both the IV-Ton ($P = 0.04$) and Sup-IV ($P = 0.04$) segments.

DISCUSSION

In the current study, the motion of the cerebellum in patients with CM-1 was examined with cardiac-gated bFFE MRI by use of a generated motion tracking software. The analysis explored separate but interrelated questions: (1) is cerebellar tonsil strain associated with CM-1 Valsalva headache; (2) does decompression surgery affect tonsillar motion; and (3) does reduced motion correlate with improved symptoms? Tonsil displacement, strain, and maximum strain rate reduced after PFD and Valsalva headache improved in a majority of patients after surgery. However, unlike a previous study,[17] no relationship was found between cerebellar tonsil strain and Valsalva headache.

Table 2. Summary of Headache Group Comparison for Each Segment

Segment	Subject Group	Displacement (mm)	Strain (%)	Minimum Strain Rate (s^{-1})	Maximum Strain Rate (s^{-1})
IV-Ton	No headache	0.38 (0.17–0.92)	1.05 (0.50–2.60)	−0.054 (−0.084 to −0.025)	0.130 (0.046–0.21)
	Headache	0.27 (0.15–0.66)	0.73 (0.40–1.96)	−0.029 (−0.083 to −0.024)	0.055 (0.033–0.10)
	Valsalva headache	0.48 (0.27–0.77)	1.25 (0.77–2.13)	−0.071 (−0.100 to −0.039)	0.091 (0.074–0.19)
Sup-Ton	No headache	0.53 (0.26–1.22)	0.85 (0.39–1.86)	−0.036 (−0.060 to −0.015)	0.085 (0.037–0.16)
	Headache	0.38 (0.19–0.90)	0.61 (0.30–1.35)	−0.024 (−0.043 to −0.015)	0.048 (0.026–0.09)
	Valsalva headache	0.67 (0.37–1.08)	0.97 (0.59–1.69)	−0.040 (−0.061 to −0.024)	0.073 (0.053–0.14)
Sup-IV	No headache	0.17 (0.13–0.28)	0.60 (0.46–0.93)	−0.031 (−0.038 to −0.022)	0.054 (0.036–0.064)
	Headache	0.16 (0.10–0.21)	0.56 (0.37–0.71)	−0.028 (−0.039 to −0.021)	0.044 (0.024–0.061)
	Valsalva headache	0.17 (0.11–0.34)	0.57 (0.37–1.05)	−0.035 (−0.054 to −0.025)	0.049 (0.035–0.081)

Results are displayed as median (interquartile range [Q1–Q3]).
IV, fastigium of the fourth ventricle; Ton, tip of the cerebellar tonsil; Sup, superior.

Table 3. Summary of Comparison Tests for Headache Type (Kruskal-Wallis Test) and Operative Status (Sign Test) for Each Segment

	P Value											
	IV-Ton				Sup-Ton				Sup-IV			
	Disp	Strain	MinSR	MaxSR	Disp	Strain	MinSR	MaxSR	Disp	Strain	MinSR	MaxSR
Headache type	0.21	0.20	0.07	0.06	0.29	0.27	0.10	0.10	0.45	0.46	0.29	0.25
Pre vs. Post	**0.003***	**0.012***	0.18	**0.04***	**0.012***	**0.012***	0.18	**0.04***	0.115	0.115	0.51	0.18

Significant comparisons are bolded (*$P < 0.05$).
IV, fastigium of the fourth ventricle; Ton, tip of the cerebellar tonsil; Sup, superior surface of the cerebellum; Disp, displacement; MinSR, minimum strain rate; MaxSR, maximum strain rate; Pre, preoperative group; Post, postoperative group; Headache type; no headache, non-Valsalva headache, Valsalva headache.

Cerebellar Tonsil Motion in CM-1

This study confirmed that cerebellar motion in patients with CM-1 is composed of both displacement and tissue strain (deformation). Tonsillar motion was quantified using metrics of displacement, tissue strain, and strain rate over 3 anatomic segments within the posterior fossa.

In vivo motion of neural structures in patients with CM-1 has been investigated by various MRI[17,21-27] and intraoperative ultrasound[28,29] techniques. Phase contrast MRI has been used in patients with CM-1 to demonstrate an increase in motion of the cerebellar tonsils,[26] the spinal cord at the foramen magnum,[25] and the rostral spinal cord,[21,22,24] compared with control groups. This technique revealed a nonsignificant trend toward increased tonsillar motion in a small sample of CM-1 patients with Valsalva headache.[26] Another study used 2D fast imaging employing steady-state acquisition (2D FIESTA), with the T2 sagittal section viewed as a cine loop, to assess tonsil motion.[23] Using this imaging technique, patients with CM-1 had significantly more motion compared with controls, but this research did not investigate associations with Valsalva headache.

However, these techniques are limited because they assess the motion of a single point across the cardiac cycle rather than the relationship and movement of 2 points. As a consequence, displacement and strain cannot be delineated. Despite this, it has been suggested that motion may predict outcome after PFD[30] and may affect the CSF fluid dynamics at the craniocervical junction.[31] Recently this issue has been overcome using the MRI technique of displacement encoding with stimulated echoes (DENSE). This has been used to investigate regional cardiac-driven brain tissue displacement and strain in healthy individuals.[32] However, widespread availability of this technique is limited in current clinical practice, and controlled research investigation of this technology in CM-1 remains in progress.[33]

bFFE is a more widely accessible alternative for the assessment of cerebellar motion. bFFE has been previously used to define displacement and strain of the cerebellar tonsils in healthy controls,[17] and the current study demonstrated an increase in displacement and strain in patients with CM-1 compared with this normal cohort.[17] Tonsil motion, including both displacement and strain, was reduced after surgery. Whereas this was evident in both the IV-Ton and Sup-Ton segments after PFD, motion localized to the IV-Ton segment was likely responsible, in as much as no difference was seen in the Sup-IV segment. Reduced tonsil motion after surgery was previously demonstrated by Leung et al.,[17] who showed that whereas motion reduces after PFD, it remains elevated above control levels.

Tissue Strain

Strain and displacement were calculated relative to tissue parameters at the start of systole. This allowed a standardized measure to compare data and avoided variation in timing acquisition between image sets. Tissue strain may contain both tension and

Table 4. Summary of Operative Group Comparison for Each Segment

Segment	Subject Group	Displacement (mm)	Strain (%)	Minimum Strain Rate (s^{-1})	Maximum Strain Rate (s^{-1})
IV-Ton	Pre	0.56 (0.31—1.02)	1.48 (0.89—2.50)	−0.14 (−0.18 to −0.07)	0.23 (0.08—0.26)
	Post	0.18 (0.13—0.33)	0.51 (0.40—0.92)	−0.04 (−0.07 to −0.03)	0.06 (0.05—0.13)
Sup-Ton	Pre	0.75 (0.36—1.23)	1.06 (0.58—1.78)	−0.08 (−0.12 to −0.04)	0.15 (0.07—0.20)
	Post	0.26 (0.21—0.44)	0.42 (0.31—0.67)	−0.02 (−0.05 to −0.017)	0.04 (0.03—0.09)
Sup-IV	Pre	0.20 (0.13—0.27)	0.69 (0.45—0.97)	−0.05 (−0.10 to −0.034)	0.07 (0.06—0.10)
	Post	0.14 (0.12—0.20)	0.47 (0.44—0.70)	−0.02 (−0.04 to −0.019)	0.04 (0.03—0.08)

Results are displayed as median (interquartile range [Q1—Q3]).
IV, fastigium of the fourth ventricle; Ton, tip of the cerebellar tonsil; Sup, superior surface of the cerebellum; Pre, preoperative group; Post, postoperative group.

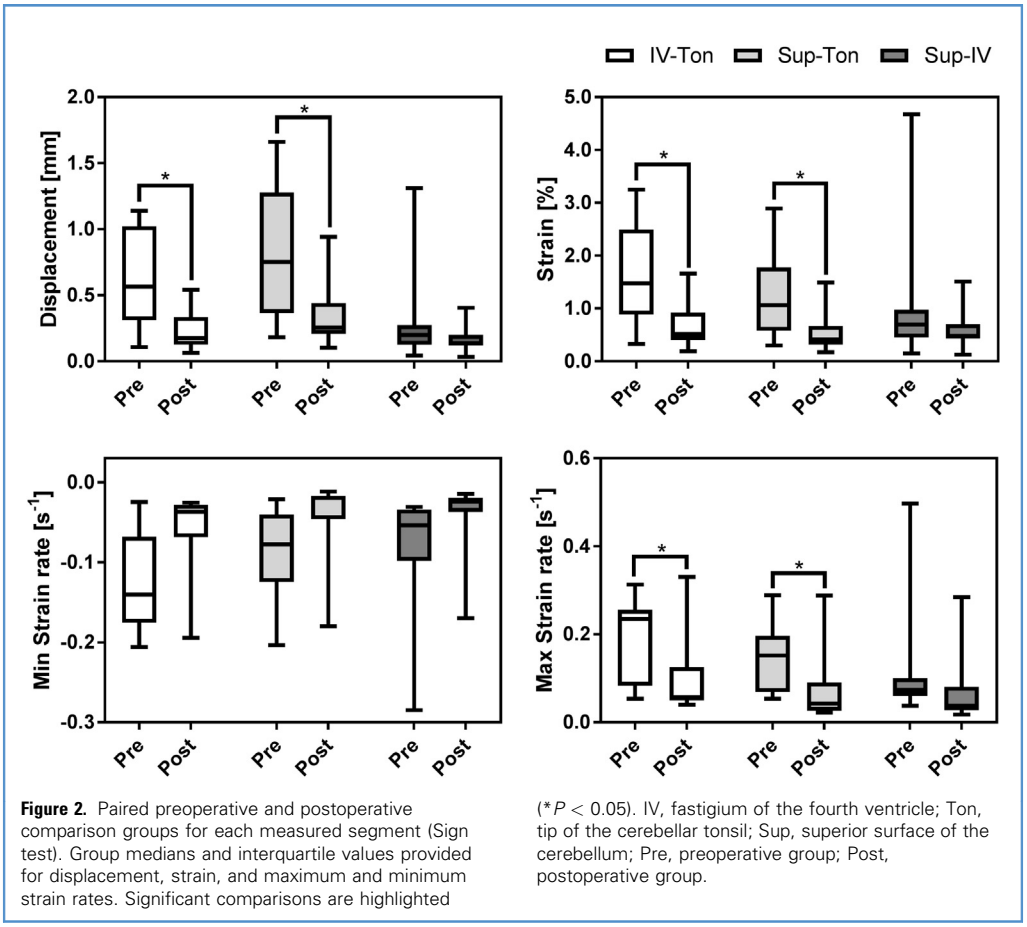

Figure 2. Paired preoperative and postoperative comparison groups for each measured segment (Sign test). Group medians and interquartile values provided for displacement, strain, and maximum and minimum strain rates. Significant comparisons are highlighted ($*P < 0.05$). IV, fastigium of the fourth ventricle; Ton, tip of the cerebellar tonsil; Sup, superior surface of the cerebellum; Pre, preoperative group; Post, postoperative group.

compression. With our methodology it is difficult to delineate the component of motion attributable to tension or compression, in as much as the "resting" unstrained length of the cerebellar tonsils is not known in vivo.

Tissue strain, particularly if chronic, may lead to changes in tissue microstructure. Diffusion tensor imaging (DTI) has been used to assess microstructural brain alterations in CM-1.[34-39] This technique in vivo, however, is limited because of the inherent motion of the neural structures, which may have an impact on accuracy. Despite this, diffusion abnormalities have been demonstrated in the brainstem,[34,36] the middle cerebellar peduncles,[35] and distant to the posterior fossa, including the corpus callosum, fornix, and basal ganglia.[34,37] There is preliminary evidence that diffusion changes within the brainstem normalize after PFD[36]; however, that study involved a small sample of CM-1 patients.

Pathogenesis of Valsalva Headache

Although the cause of CM-1–associated Valsalva headache is not understood, various theories have been proposed.[3,9-13] In the current study, tissue strain of neural structures at the craniocervical junction was hypothesized to contribute to the pathogenesis of Valsalva headache. Previous findings have suggested a correlation between strain and Valsalva headache occurring in patients at rest.[17] These findings suggest that the behavior of tissue motion is the same at rest and during Valsalva maneuvers, when the patient is symptomatic. Therefore, in the current study, strain occurring during the cardiac cycle was used as a surrogate of strain during Valsalva maneuvers. However, the veracity of this assumption remains in doubt.

Effect of Valsalva Maneuvers on Cerebellar Motion

The current study did not find a relationship between tonsillar motion (including both tissue strain and tissue displacement) and Valsalva headache in patients at rest. Invasive techniques have shown that Valsalva maneuvers cause only transient changes in intracranial CSF pressure.[40] We postulate that this may affect cerebellar motion in CM-1. Additionally, the time-limited impact of Valsalva maneuvers is consistent with the transient nature of Valsalva headache symptoms. Our study examined only cardiac cycle–related motion and did not directly examine the effect of Valsalva maneuvers.

The assessment of the effects of Valsalva on cerebellar motion and CSF flow has been limited by noninvasive imaging techniques. Long acquisition times for a rapid physiologic change have limited the applicability of cine MRI for Valsalva maneuvers.

Bhadella et al.[41] used fast cine-PC and pencil beam imaging to demonstrate in healthy patients that CSF displacement volume and the absolute flow at the craniocervical junction reduced during a Valsalva maneuver and increased immediately before returning to baseline. This technique was recently replicated in patients with CM-1, revealing a reduced CSF stroke volume during a Valsalva maneuver.[42]

The effects of Valsalva on cerebellar motion are yet to be explored in CM-1. This represents an interesting area for further evaluation with emerging real-time MRI techniques and intraoperative ultrasound. However, researchers in this field will also need to address the challenge of how to achieve a reproducible and consistent Valsalva effect in patients who are often symptomatic with such maneuvers.

Limitations

The results of this study are limited by several factors. The study population was a cross-sectional cohort of patients from a single neurosurgical center, and only patients who underwent bFFE imaging were included. This introduces potential selection bias and may not be representative of the general CM-1 population. This is compounded by the proportion of patients excluded from analysis because of poor image quality.

Clinical assessment of patients was performed by the treating clinicians, who were not blinded to their care. Furthermore, all data used in the current study were retrospectively extracted from medical records, and previous inaccuracies in the gathering and recording of clinical information can affect the subsequent analysis undertaken.

CM-1 commonly presents with a spectrum of symptoms. For the purposes of this study, non-Valsalva and Valsalva headache were dichotomized into present or absent. However, owing to the retrospective nature of the study, the classification of headache across cases may not be consistent. In addition, the binary classification does not fully reflect the range of symptoms experienced by patients and may have affected the findings of this study. This could be addressed in future studies with the use of a standardized assessment tool.

The indication for surgery was individualized, and whereas surgical patients were symptomatic and their symptoms had not yielded to conservative measures, the ultimate decision to proceed to surgery was made in combination with the patient's wishes, not always using defined objective markers. This limits the ability to use surgery as a surrogate for disease severity, but it also highlights the need for an objective measure supporting a role for surgery and to assess the technical outcomes of surgery.

Finally, bFFE assessment of tissue motion is limited because it applies a 1-dimensional solution to a 3-dimensional problem. This requires the motion metrics of displacement, strain, and strain rate to be uniform and may lead to a failure to identify-region specific differences. This may be overcome by techniques that use 2-dimensional techniques.

CONCLUSION

bFFE MRI analysis provides novel insights into the pathophysiology of symptomatic CM-1, and it offers multiple biomarkers of change associated with neurosurgical intervention. The relationship between tonsillar motion and Valsalva headache in CM-1 remains to be elucidated, and likely requires MRI sequence acquisition during Valsalva maneuvers using techniques possessing higher temporal resolution. Continued investigation of tonsillar strain and displacement parameters is nevertheless worthwhile as part of ongoing efforts to improve understanding of the causes, management, and outcomes of CM-1.

REFERENCES

1. Elster AD, Chen MY. Chiari I malformations: clinical and radiologic reappraisal. *Radiology*. 1992;183:347-353.
2. Meadows J, Kraut M, Guarnieri M, Haroun RI, Carson BS. Asymptomatic Chiari type I malformations identified on magnetic resonance imaging. *J Neurosurg*. 2000;92:920-926.
3. Milhorat TH, Chou MW, Trinidad EM, et al. Chiari I malformation redefined: clinical and radiographic findings for 364 symptomatic patients. *Neurosurgery*. 1999;44:1005-1017.
4. Smith BW, Strahle J, Bapuraj JR, Muraszko KM, Garton HJ, Maher CO. Distribution of cerebellar tonsil position: Implications for understanding Chiari malformation. *J Neurosurg*. 2013;119:812-819.
5. Sekula RF Jr, Jannetta PJ, Casey KF, Marchan EM, Sekula LK, McCrady CS. Dimensions of the posterior fossa in patients symptomatic for Chiari I malformation but without cerebellar tonsillar descent. *Cerebrospinal Fluid Res*. 2005;2:11.
6. Barkovich AJ, Wippold FJ, Sherman JL, Citrin CM. Significance of cerebellar tonsillar position on MR. *AJNR Am J Neuroradiol*. 1986;7:795-799.
7. Bejjani GK. Definition of the adult Chiari malformation: a brief historical overview. *Neurosurg Focus*. 2001;11:E1.
8. Stevens JM, Serva WA, Kendall BE, Valentine AR, Ponsford JR. Chiari malformation in adults: Relation of morphological aspects to clinical features and operative outcome. *J Neurol Neurosurg Psychiatry*. 1993;56:1072-1077.
9. Pascual J, Oterino A, Berciano J. Headache in type I Chiari malformation. *Neurology*. 1992;42:1519-1521.
10. Edmeads J. The cervical spine and headache. *Neurology*. 1988;38:1874-1878.
11. Williams B. Cough headache due to craniospinal pressure dissociation. *Arch Neurol*. 1980;37:226-230.
12. Stovner LJ. Headache associated with the Chiari type I malformation. *Headache*. 1993;33:175-181.
13. Sansur CA, Heiss JD, DeVroom HL, Eskioglu E, Ennis R, Oldfield EH. Pathophysiology of headache associated with cough in patients with Chiari I malformation. *J Neurosurg*. 2003;98:453-458.
14. Clarke EC, Stoodley MA, Bilston LE. Changes in temporal flow characteristics of CSF in Chiari malformation type I with and without syringomyelia: Implications for theory of syrinx development. *J Neurosurg*. 2013;118:1135-1140.
15. Clarke EC, Fletcher DF, Stoodley MA, Bilston LE. Computational fluid dynamics modelling of cerebrospinal fluid pressure in Chiari malformation and syringomyelia. *J Biomech*. 2013;46:1801-1809.
16. Lloyd RA, Fletcher DF, Clarke EC, Bilston LE. Chiari malformation may increase perivascular cerebrospinal fluid flow into the spinal cord: a subject-specific computational modelling study. *J Biomech*. 2017;65:185-193.
17. Leung V, Magnussen JS, Stoodley MA, Bilston LE. Cerebellar and hindbrain motion in Chiari malformation with and without syringomyelia. *J Neurosurg Spine*. 2016;24:546-555.
18. Sharma A, Parsons MS, Pilgram TK. Balanced steady-state free-precession MR imaging for measuring pulsatile motion of cerebellar tonsils during the cardiac cycle: a reliability study. *Neuroradiology*. 2012;54:133-138.
19. Radmanesh A, Greenberg JK, Chatterjee A, Smyth MD, Limbrick DD Jr, Sharma A. Tonsillar

pulsatility before and after surgical decompression for children with Chiari malformation type 1: an application for true fast imaging with steady state precession. *Neuroradiology*. 2015;57:387-393.

20. Li AE, Wilkinson MD, McGrillen KM, Stoodley MA, Magnussen JS. Clinical applications of cine balanced steady-state free precession mri for the evaluation of the subarachnoid spaces. *Clin Neuroradiol*. 2015;25:349-360.

21. Alperin N, Loftus JR, Oliu CJ, et al. Magnetic resonance imaging measures of posterior cranial fossa morphology and cerebrospinal fluid physiology in Chiari malformation type I. *Neurosurgery*. 2014;75:515-522 [discussion: 522].

22. Alperin N, Sivaramakrishnan A, Lichtor T. Magnetic resonance imaging-based measurements of cerebrospinal fluid and blood flow as indicators of intracranial compliance in patients with Chiari malformation. *J Neurosurg*. 2005;103:46-52.

23. Cousins J, Haughton V. Motion of the cerebellar tonsils in the foramen magnum during the cardiac cycle. *AJNR Am J Neuroradiol*. 2009;30:1587-1588.

24. Hofmann E, Warmuth-Metz M, Bendszus M, Solymosi L. Phase-contrast MR imaging of the cervical CSF and spinal cord: Volumetric motion analysis in patients with Chiari I malformation. *AJNR Am J Neuroradiol*. 2000;21:151-158.

25. Lawrence BJ, Luciano M, Tew J, et al. Cardiac-related spinal cord tissue motion at the foramen magnum is increased in patients with type I Chiari malformation and decreases postdecompression surgery. *World Neurosurg*. 2018;116:e28-e307.

26. Pujol J, Roig C, Capdevila A, et al. Motion of the cerebellar tonsils in Chiari type I malformation studied by cine phase-contrast MRI. *Neurology*. 1995;45:1746-1753.

27. Yiallourou TI, Kroger JR, Stergiopulos N, Maintz D, Martin BA, Bunck AC. Comparison of 4D phase-contrast MRI flow measurements to computational fluid dynamics simulations of cerebrospinal fluid motion in the cervical spine. *PLoS One*. 2012;7:e52284.

28. Oldfield EH, Muraszko K, Shawker TH, Patronas NJ. Pathophysiology of syringomyelia associated with Chiari I malformation of the cerebellar tonsils: Implications for diagnosis and treatment. *J Neurosurg*. 1994;80:3-15.

29. Jokich PM, Rubin JM, Dohrmann GJ. Intraoperative ultrasonic evaluation of spinal cord motion. *J Neurosurg*. 1984;60:707-711.

30. Alperin N, Loftus JR, Bagci AM, et al. Magnetic resonance imaging-based measures predictive of short-term surgical outcome in patients with Chiari malformation Type I: a pilot study. *J Neurosurg Spine*. 2017;26:28-38.

31. Pahlavian SH, Loth F, Luciano M, Oshinski J, Martin BA. Neural tissue motion impacts cerebrospinal fluid dynamics at the cervical medullary junction: a patient-specific moving-boundary computational model. *Ann Biomed Eng*. 2015;43:2911-2923.

32. Pahlavian SH, Oshinski J, Zhong X, Loth F, Amini R. Regional quantification of brain tissue strain using displacement-encoding with stimulated echoes magnetic resonance imaging. *J Biomech Eng*. 2018;140.

33. Oshinski J, Pahlavian S, Schuster J, et al. *Motion of the cerebellum in patients with Chiari malformation compared to healthy subjects: A quantitative study using spiral cine DENSE MRI*. France: ISMRM; 2018.

34. Kurtcan S, Alkan A, Yetis H, et al. Diffusion tensor imaging findings of the brainstem in subjects with tonsillar ectopia. *Acta Neurolog Belg*. 2018;118:39-45.

35. Eshetu T, Meoded A, Jallo GI, Carson BS, Huisman TA, Poretti A. Diffusion tensor imaging in pediatric Chiari type I malformation. *Dev Med Child Neurol*. 2014;56:742-748.

36. Krishna V, Sammartino F, Yee P, et al. Diffusion tensor imaging assessment of microstructural brainstem integrity in Chiari malformation type I. *J Neurosurg*. 2016;125:1112-1119.

37. Kumar M, Rathore RK, Srivastava A, Yadav SK, Behari S, Gupta RK. Correlation of diffusion tensor imaging metrics with neurocognitive function in Chiari I malformation. *World Neurosurg*. 2011;76:189-194.

38. Alexander AL, Hurley SA, Samsonov AA, et al. Characterization of cerebral white matter properties using quantitative magnetic resonance imaging stains. *Brain Connect*. 2011;1:423-446.

39. Lin M, He H, Schifitto G, Zhong J. Simulation of changes in diffusion related to different pathologies at cellular level after traumatic brain injury. *Magn Reson Med*. 2016;76:290-300.

40. Williams B. Simultaneous cerebral and spinal fluid pressure recordings. 2. Cerebrospinal dissociation with lesions at the foramen magnum. *Acta Neurochir (Wien)*. 1981;59:123-142.

41. Bhadelia RA, Patz S, Heilman C, et al. Cough-associated changes in CSF flow in Chiari I malformation evaluated by real-time MRI. *AJNR Am J Neuroradiol*. 2016;37:825-830.

42. Bezuidenhout AF, Khatami D, Heilman CB, et al. Relationship between cough-associated changes in CSF flow and disease severity in Chiari I malformation: an exploratory study using real-time MRI. *AJNR Am J Neuroradiol*. 2018;39:1267-1272.

Conflict of interest statement: The study was supported by a grant from the Column of Hope.

Received 30 December 2018; accepted 24 May 2019

Citation: World Neurosurg. (2019) 130:e74-e81.
https://doi.org/10.1016/j.wneu.2019.05.211

Journal homepage: ***www.journals.elsevier.com/world-neurosurgery***

Available online: ***www.sciencedirect.com***